Ce(III) containing tricobalt-substituted silico-tungstate $[CeCo_3Si_2W_{20}O_{74}(NO_3)(OH)(H_2O)]^{13-}$: A versatile nano-cluster with a multitude of applications

*Shivani,[a] Vivek Das, [a,b]Ahsan ul haq,[a] Shivangi Prandiyal,[c] Anwar Alam,[c] Anne-Lucie Teillout,[d] Pedro de Oliveira,[d] Arun Kant,[e] Himani Chahar,[f] Debabrata Mishra,[f] Olivier Blacque,[g] Firasat Hussain[a] **

Table of Contents

Table S1. Crystal data and structure refinement for **La-1a** and **Ce-2a**……..……**S4**

Table S2. Crystal data and structure refinement for **Pr-3a** and **Nd-4a**……..……**S5**

Table S3. Dye Degradation Performance of 3d-4f Heterometallic Silicotungstates and Related POMs……**S6**

Table S4. IC_{50} value of reported Polyoxotungstates (POTS) on different cancer cell Lines - Cytotoxicity Data……...**S7**

Table S5. Average overpotential at -10 mA/cm^2 for different electrode materials…….....**S8**

Figure S1. Ball-and-stick representation of polyanion **$[LnCo_3Si_2W_{20}O_{74}(NO_3)(OH)(H_2O)]^{13-}$ (1a-4a)**.....**S9**

Figure S2. [A] FT-IR spectra of the nanoclusters **(1a-4a);** [B] Spectral Comparison of **(SiW_9O_{34})** Ligand and **1a**……..**S10**

Figure S3. Thermogravimetric analysis curve of the complexes **(1a- 14a)**……..**S11**

Figure S4. CVs recorded at a scan rate of 100 mV.s^{-1}, with a POM concentration of 0.2 mM in 0.5 M Li_2SO_4 + H_2SO_4 / pH 3.00, at two different reverse potentials. [A] La **(1a)** [B] Pr **(3a)** [C] Nd **(4a)**.....**S13**

Figure S5. CVs recorded at a scan rate of 100 mV.s^{-1}, with a POM concentration of 0.2 mM in 1.0 M $LiCH_3COO.2H_2O$ + CH_3COOH / pH 5.00, for all the POMs in the series studied individually……..**S14**

Figure S6. CVs recorded at a scan rate of 100 mV.s^{-1} for all the POMs in the series, studied individually at a concentration of 0.2 mM, in 0.5 M Li_2SO_4 + H_2SO_4 / pH 3.00 and in 1.0 M $LiCH_3COO.2H_2O$ + CH_3COOH / pH 5.00.....**S15**

Figure S7. CVs recorded at a scan rate of 100 mV.s^{-1} for all the POMs in the series, studied individually at a concentration of 0.2 mM, in (A) 0.5 M Li_2SO_4 + H_2SO_4 / pH 3.00 and in (B) 1.0 M $LiCH_3COO.2H_2O$ + CH_3COOH / pH 5.00.....**S16**

Figure S8. CVs recorded at a scan rate of 10 mV.s^{-1} for all the POMs in the series, studied individually at a concentration of 0.2 mM, in 1.0 M $LiCH_3COO.2H_2O$ + CH_3COOH / pH 5.00..**S17**

Figure S9. CVs recorded at a scan rate of 100 mV.s^{-1} with La- **(1a)** [blue] and with Pr- **(3a)** [green], studied individually at a concentration of 0.2 mM, in 0.5 M Li_2SO_4 + H_2SO_4 / pH 3.00. (A) Initial scan direction towards the positive potentials. (B) Initial scan direction towards the negative potentials.....**S18**

Figure S10. Proposed Mechanism of Photocatalytic dye degradation……**S19**

Figure S11. Linear sweep voltammograms for Ce-based POM catalyst in 0.5 M KCl (black), 0.5 M H_2SO_4 (Red), and 0.5 M Na_2SO_4 (Blue)……..……..**S20**

Figure S12. The molecular structures of polyanions (**1a-4a**) shown without cations (Cs^+, K^+) and isolated water molecules. Displacement ellipsoids are drawn at the 30% probability level……...……..**S21**

References……...**S23**

Table S1. Crystal data and structure refinement for La-1a and Ce-2a

Identification code	**La-1a**	**Ce-2a**
CCDC number	2518417	2518416
Empirical formula	$Co_3Cs_{0.75}H_{43}K_{12.25}LaNO_{99}Si_2W_{20}$	$CeCo_3Cs_{0.75}H_3K_{12.25}NO_{99}Si_2W_{20}$
Formula weight	6268.89	6270.10
Temperature/K	150.00(10)	149.94(15)
Crystal system	triclinic	triclinic
Space group	P-1	P-1
a/Å	11.67157(9)	11.66600(10)
b/Å	12.44186(11)	12.42430(10)
c/Å	36.1804(2)	36.1689(3)
α/°	90.7046(6)	90.7070(10)
β/°	97.6008(6)	97.7140(10)
γ/°	116.1071(8)	116.0880(10)
Volume/Å^3	4661.78(7)	4650.66(8)
Z	2	2
ρ_{calc}g/cm^3	4.466	4.478
μ/mm^{-1}	26.510	26.603
F(000)	5524.0	5526.0
Crystal size/mm^3	0.22 × 0.12 × 0.03	0.29 × 0.12 × 0.03
Radiation	Mo Kα (λ = 0.71073)	Mo Kα (λ = 0.71073)
2Θ range for data collection/°	4.232 to 52.744	4.45 to 52.744
Index ranges	$-14 \le h \le 14$, $-15 \le k \le 15$, $-45 \le l \le 45$	$-14 \le h \le 14$, $-15 \le k \le 15$, $-45 \le l \le 45$
Reflections collected	115428	114560
Independent reflections	19071 [R_{int} = 0.0360, R_{sigma} = 0.0199]	19029 [R_{int} = 0.0339, R_{sigma} = 0.0210]
Data/restraints/parameters	19071/296/1373	19029/301/1390
Goodness-of-fit on F^2	1.245	1.205
Final R indexes [I>=2σ (I)]	R_1 = 0.0342, wR_2 = 0.0746	R_1 = 0.0374, wR_2 = 0.0825
Final R indexes [all data]	R_1 = 0.0355, wR_2 = 0.0751	R_1 = 0.0396, wR_2 = 0.0834
Largest diff. peak/hole / e Å^{-3}	4.70/-1.76	4.07/-2.23

Table S2. Crystal data and structure refinement for Pr-3a and Nd-4a

Identification code	**Pr-3a**	**Nd-4a**
CCDC number	2518418	2518805
Empirical formula	$Co_3Cs_{0.75}H_3K_{12.25}NO_{99}PrSi_2W_{20}$	$Co_3Cs_{0.75}H_3K_{12.25}NNdO_{99}Si_2W_{20}$
Formula weight	6270.89	6274.22
Temperature/K	150.00(10)	150.00(10)
Crystal system	triclinic	triclinic
Space group	P-1	P-1
a/Å	11.69060(10)	11.69490(10)
b/Å	12.46520(10)	12.4491(2)
c/Å	36.2275(2)	36.2187(4)
α/°	90.7940(10)	90.6260(10)
β/°	97.7140(10)	97.9330(10)
γ/°	116.1050(10)	116.0320(10)
Volume/Å^3	4682.03(7)	4677.64(11)
Z	2	2
ρ_{calc}g/cm^3	4.448	4.455
μ/mm^{-1}	26.459	26.518
F(000)	5528.0	5530.0
Crystal size/mm^3	0.15 × 0.09 × 0.03	0.44 × 0.15 × 0.04
Radiation	Mo Kα (λ = 0.71073)	Mo Kα (λ = 0.71073)
2Θ range for data collection/°	4.44 to 52.744	4.25 to 52.742
Index ranges	-14 ≤ h ≤ 14, -15 ≤ k ≤ 15, -45 ≤ l ≤ 45	-14 ≤ h ≤ 14, -15 ≤ k ≤ 15, -45 ≤ l ≤ 45
Reflections collected	137231	93044
Independent reflections	19147 [R_{int} = 0.0290, R_{sigma} = 0.0164]	19120 [R_{int} = 0.0534, R_{sigma} = 0.0327]
Data/restraints/parameters	19147/260/1367	19120/289/1385
Goodness-of-fit on F^2	1.252	1.187
Final R indexes [I>=2σ (I)]	R_1 = 0.0333, wR_2 = 0.0746	R_1 = 0.0472, wR_2 = 0.1091
Final R indexes [all data]	R_1 = 0.0343, wR_2 = 0.0749	R_1 = 0.0508, wR_2 = 0.1106
Largest diff. peak/hole / e Å^{-3}	5.54/-2.30	4.69/-1.95

Table S3. Dye Degradation Performance of 3d-4f Heterometallic Silicotungstates and Related POMs.

S. No.	Dye	Polyoxometalate Catalyst	Removal	Time (Min)	Year	Ref.
1	Congo Red (CR)	$K_8[\alpha\text{-}SiW_{11}O_{39}]$	98.6	120	2025	[1]
2	Methylene Blue(MB)	$K_4[\alpha\text{-}SiW_{12}O_{40}]$	98.4	120	2025	[1]
3	Methylene blue (MB)	SiW_9V_3@MIL-101(Cr)	100	12	2025	[2]
4	Rhodamine (RhB)	SiW_9V_3@MIL-101(Cr)	100	18	2025	[2]
5	Methylene blue (MB)	$[Cu(bte)_2(H_2O)]_2[SiMo_{12}O_{40}]\cdot 2H_2O$ (bte = 1,2-bis(1,2,4-triazol-1-yl)ethane)	84.58	160	2025	[3]
6	Methylene blue (MB)	$[Cu(btb)_2]_2[SiMo_{12}O_{40}]\cdot H_2O$ (btb = 1,4-bis(1,2,4-triazol-1-yl)butane))	96.96	160	2025	[3]
7	Rhodamine B (RhB)	$ZnO/Ag_4SiW_{12}O_{40}$(ZnO/AgSiW)	92.30%	60	2022	[4]
8	Methylene blue (MB)	SiW_{12}/MCM-22	95%	60	2021	[5]
9	Crystal violet (CV)	SiW_{12}/MCM-22	90%	60	2021	[5]
10	Methylene blue (MB)	$\{[Co_4(L)_2(HCOO)_2(OH)_2][SiO_4(W_3O_9)_4]\}\cdot 6DMF\cdot 5H_2O$ [resorcin[4]arene ligand (L)]	87.2	48h	2018	[6]
11	Methylene blue (MB)	$\{[Zn_4(L)_2(HCOO)_2(OH)_2][SiO_4(W_3O_9)_4]\}\cdot 6DMF\cdot 5H_2O$ [resorcin[4]arene ligand (L)]	67.3	48h	2018	[6]
12	Neutral red (NR)	$\{[Zn_4(L)_2(HCOO)_2(OH)_2][SiO_4(W_3O_9)_4]\}\cdot 6DMF\cdot 5H_2O$ [resorcin[4]arene ligand (L)]	80	48h	2018	[6]

Table S4. IC_{50} value of reported Polyoxotungstates (POTS) on different cancer cell Lines - Cytotoxicity Data

POM Formula/Abbreviation	**Cancer Cell Line**	**IC_{50} (72h)**	**Ref.**
$[Co(H_2O)_6\{CoSb_6O_4(H_2O)_3[Co(hmta)SbW_8O_{31}]_3\}]^{13-}$	A2780 (ovarian)	0.77 μM	[7]
Same compound	A2780cis (cisplatin-resistant)	4.35 μM	[7]
Same compound	A549 (lung)	12.65 μM	[7]
Same compound	OVCAR-3 (ovarian)	1.78 μM	[7]
Same compound	MCF-7 (breast)	12.24 μM	[7]
$C_{25}N_{10}Na_{0.7}Co_{5.3}O_{76}Sb_2W_{18}$	AGS (gastric)	**1.**42 μM	[8]
$\{Sb_8W_{36}\}$	BGC-823 (gastric)	8.68 μM	[8]
PAC-320 ($(\{(n\text{-}Bu)Sn(OH)\}_3GeW_9O_{34}]^{4-}$)	DU145 (prostate)	4.55 μM	[9]
PAC-320	LNCaP (prostate)	5.64 μM	[9]
PW_9Cu ($K_7Na_3[Cu_4(H_2O)_2(PW_9O_{34})_2]\cdot 20H_2O$)	MG-63 (osteosarcoma)	22.00 μM (48h)	[[10]

Table S5. Average overpotential at -10 mA/cm^2 for different electrode materials

Electrode Name	**Average Overpotential @ -10 mA/cm^2**
GC	1.30 ± 0.02
Ligand	1.32 ± 0.02
Pr	1.23 ± 0.02
Nd	1.16 ± 0.01
La	1.15 ± 0.01
Ce	1.11 ± 0.03

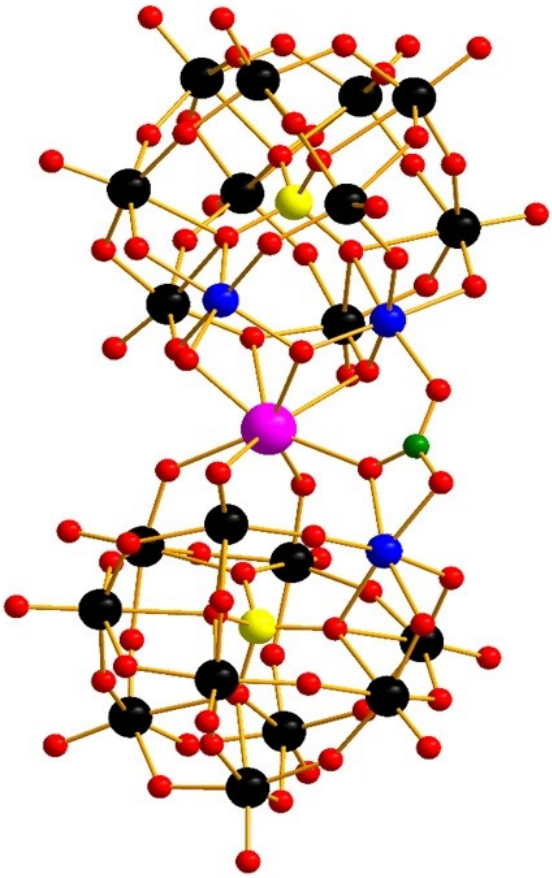

Figure S1. Ball and stick representation of polyanion **$[LnCo_3Si_2W_{20}O_{74}(NO_3)(OH)(H_2O)]^{13-}$.** (Colour code: Si = yellow sphere, W = black sphere, Ln = pink sphere, O = red sphere, Co = blue sphere, N = sea green sphere).

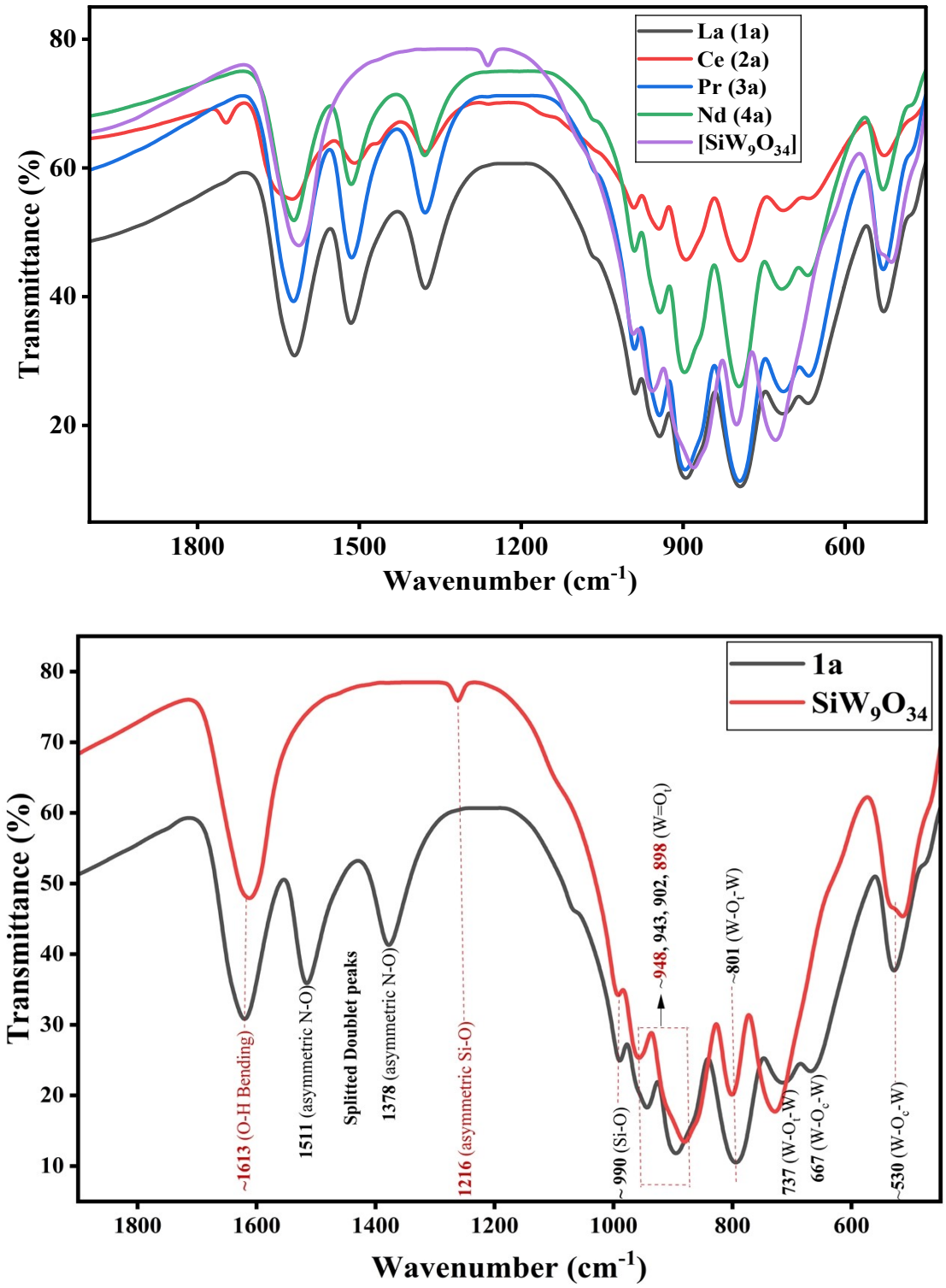

Figure S2. [A] The FT-IR spectra of the nanoclusters **(1a-4a)** (recorded on the KBr pellets). [B] Spectral Comparison of **(SiW_9O_{34})** Ligand and **1a**

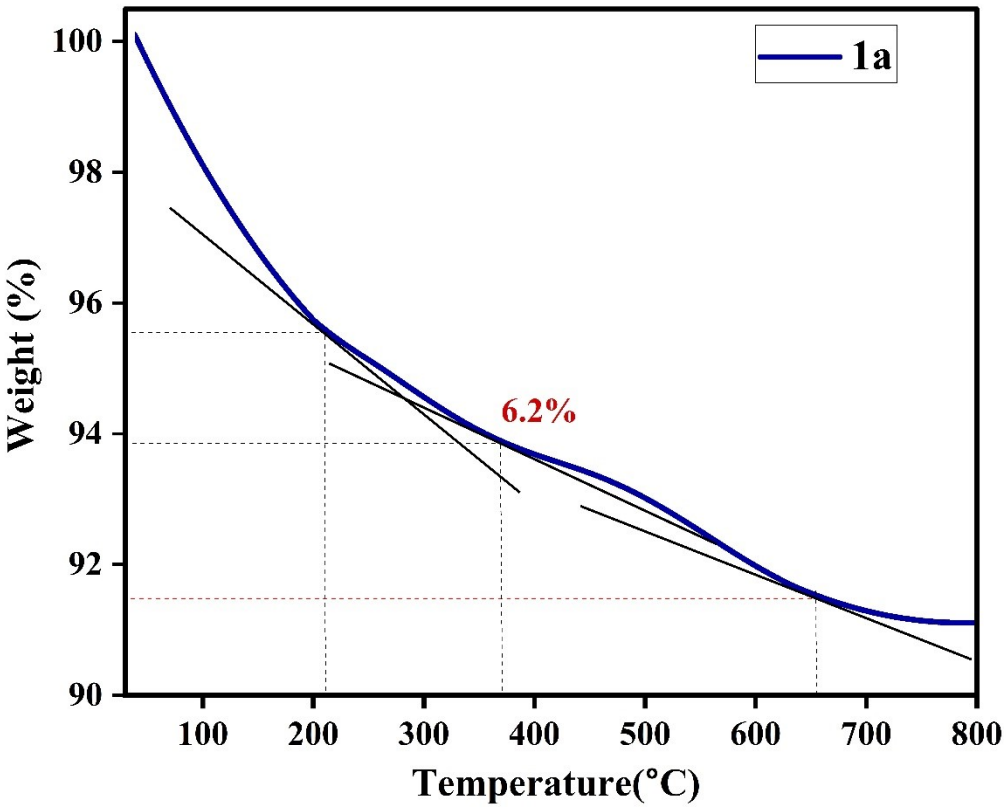
1a
100
98
96
94
92
90
Weight (%)
6.2%
100
200
300
400
500
600
700
800
Temperature(°C)

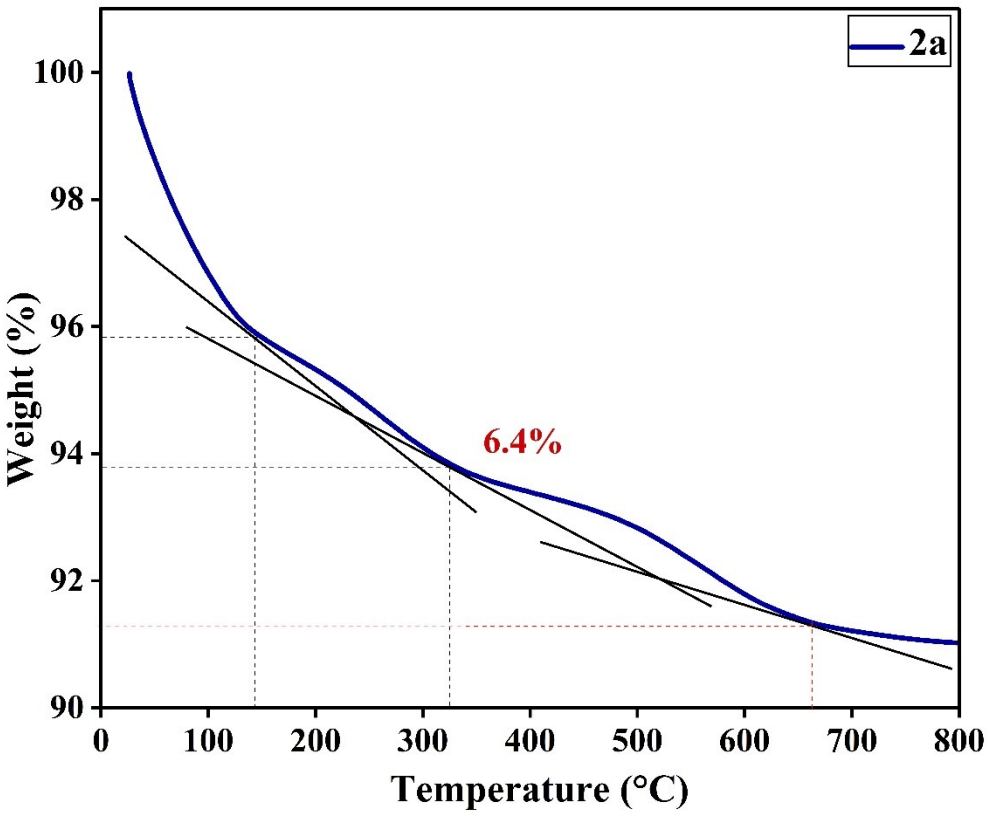
2a
100
98
96
94
92
90
Weight (%)
6.4%
0
100
200
300
400
500
600
700
800
Temperature (°C)

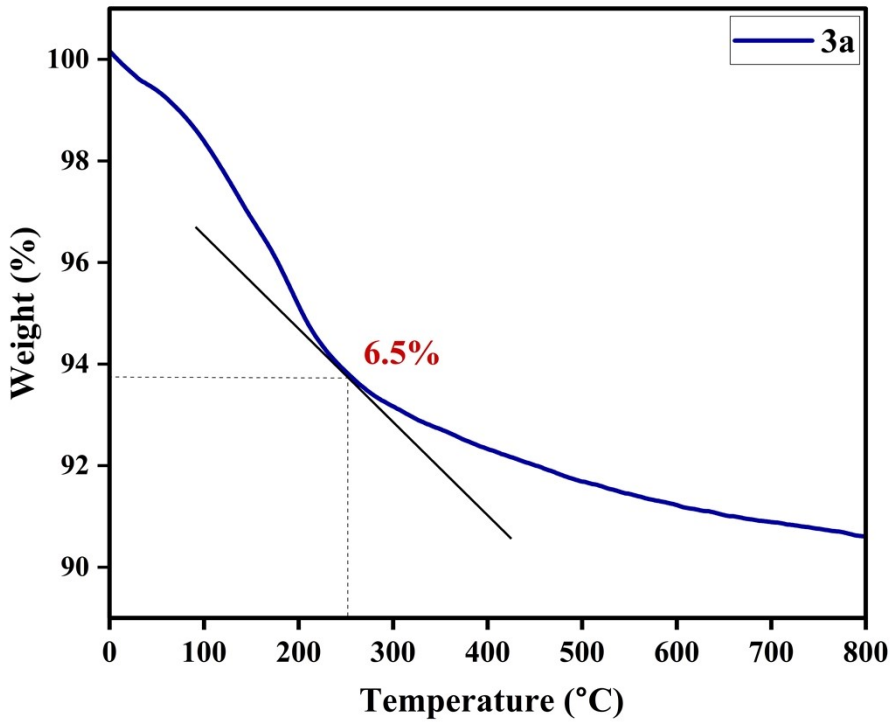
3a
100
98
96
94
92
90
Weight (%)
6.5%
0
100
200
300
400
500
600
700
800
Temperature (°C)

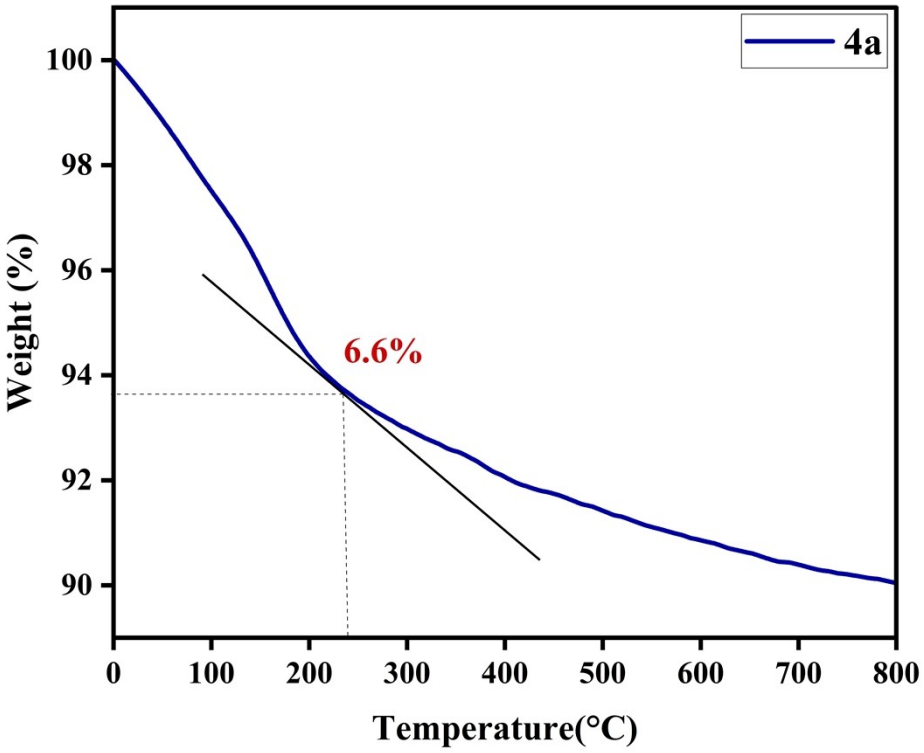
4a
100
98
96
94
92
90
Weight (%)
6.6%
0
100
200
300
400
500
600
700
800
Temperature(°C)

Figure S3. Thermogravimetric analysis curve of the complexes **$[LnCo_3Si_2W_{20}O_{74}(NO_3)(OH)(H_2O)]^{13-}$ (1a-4a).** Here, Ln = La^{III} (**1a**), Ce^{III} (**2a**), Pr^{III} (**3a**), Nd^{III} (**4a**).

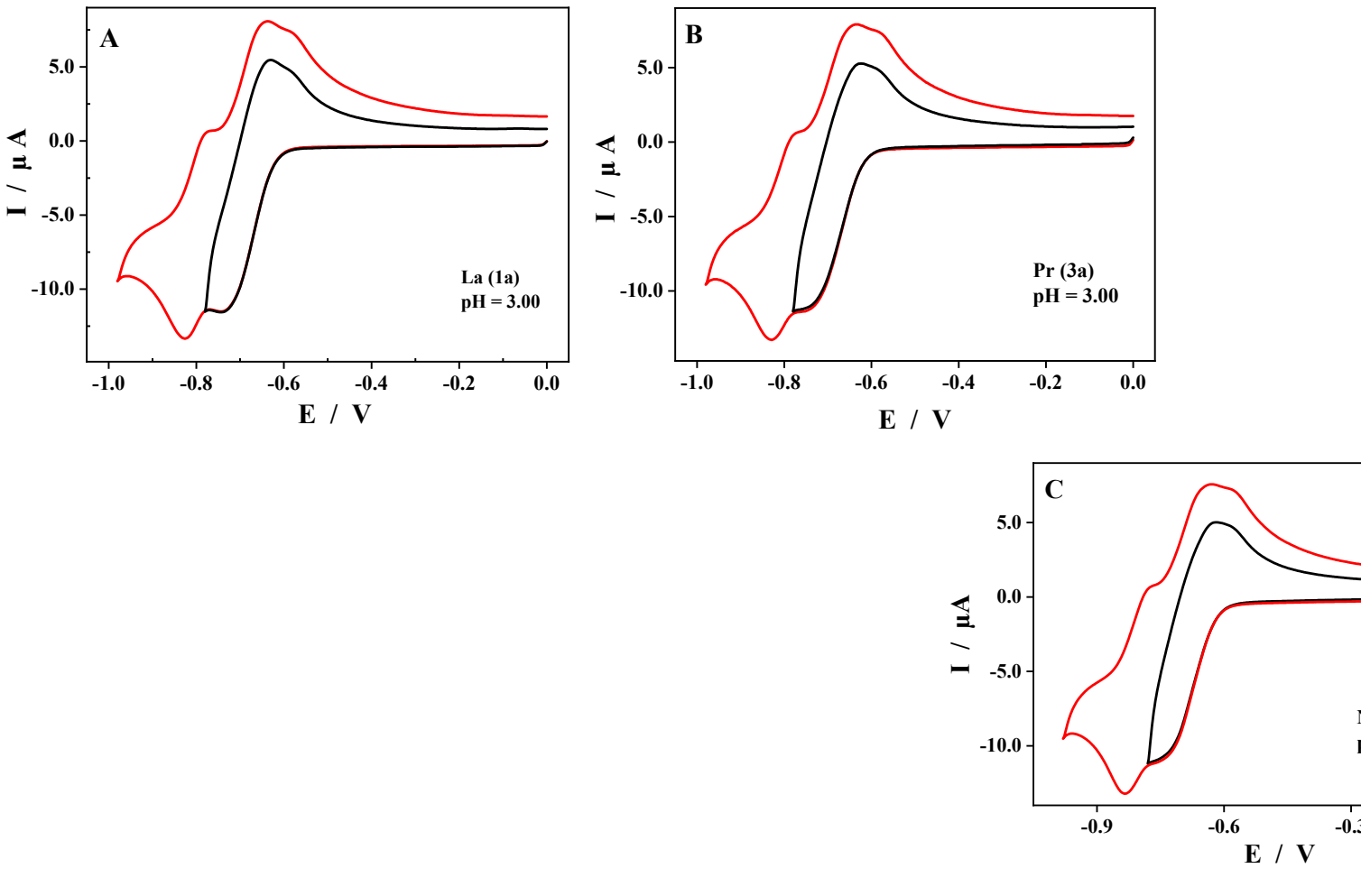

Figure S4. CVs recorded at a scan rate of 100 $mV.s^{-1}$, with a POM concentration of 0.2 mM in 0.5 M Li_2SO_4 + H_2SO_4 / pH 3.00, at two different reverse potentials. [A] La **(1a)** [B] Pr **(3a)** [C] Nd **(4a).**

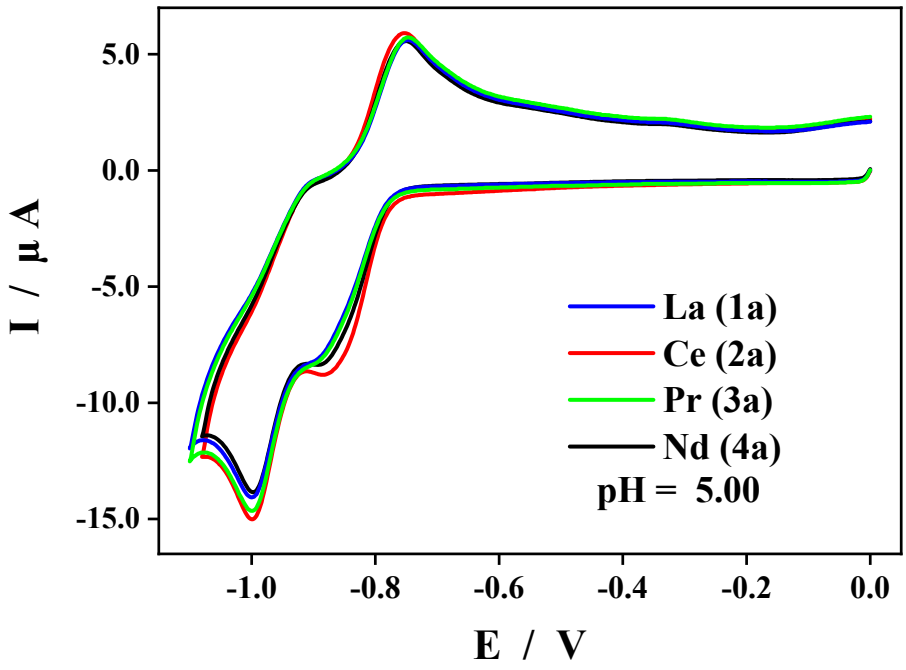

Figure S5. CVs recorded at a scan rate of 100 $mV.s^{-1}$, with a POM concentration of 0.2 mM in 1.0 M $LiCH_3COO.2H_2O$ + CH_3COOH / pH 5.00, for all the POMs in the series studied individually.

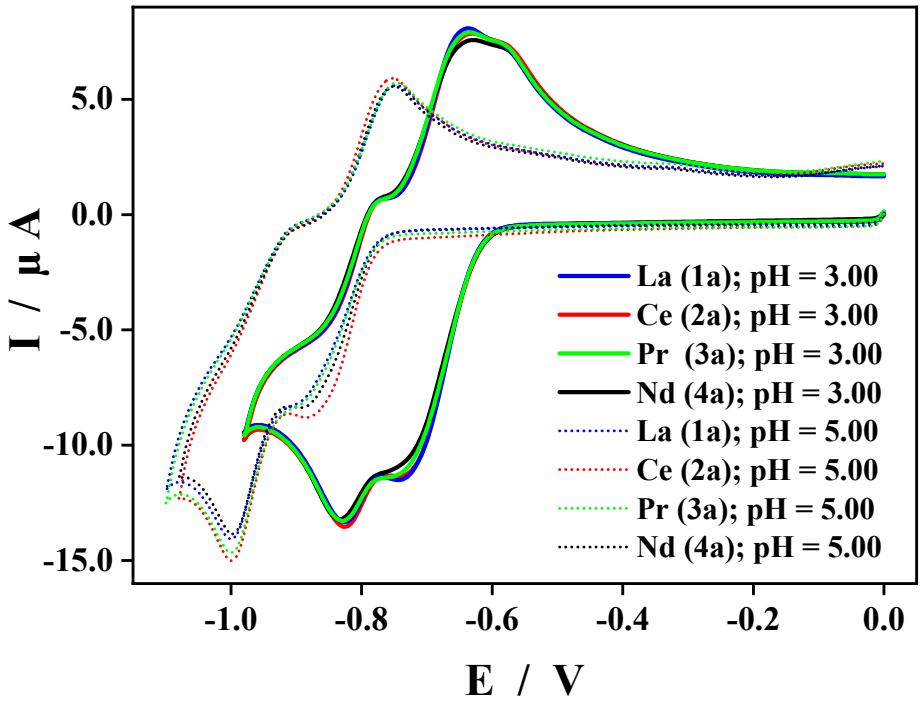

Figure S6. CVs recorded at a scan rate of 100 $mV.s^{-1}$ for all the POMs in the series, studied individually at a concentration of 0.2 mM, in 0.5 M Li_2SO_4 + H_2SO_4 / pH 3.00 and in 1.0 M $LiCH_3COO.2H_2O$ + CH_3COOH / pH 5.00.

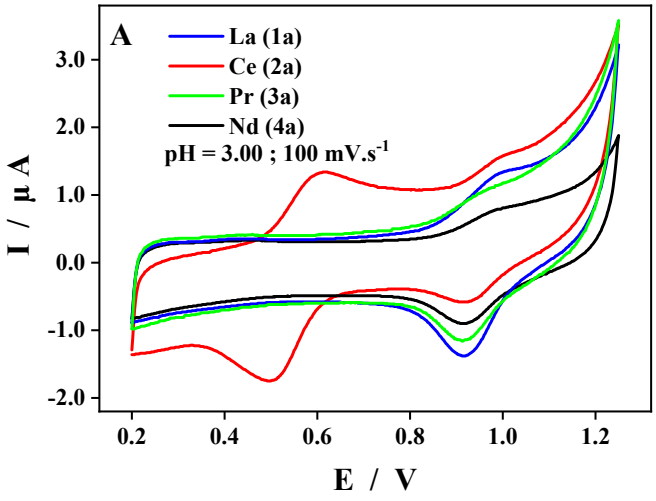

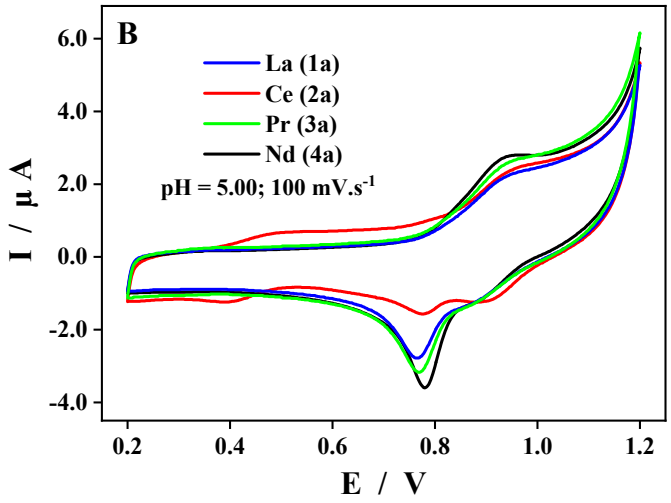

Figure S7. CVs recorded at a scan rate of 100 $mV.s^{-1}$ for all the POMs in the series, studied individually at a concentration of 0.2 mM, in (A) 0.5 M Li_2SO_4 + H_2SO_4 / pH 3.00 and in (B) 1.0 M $LiCH_3COO.2H_2O$ + CH_3COOH / pH 5.00.

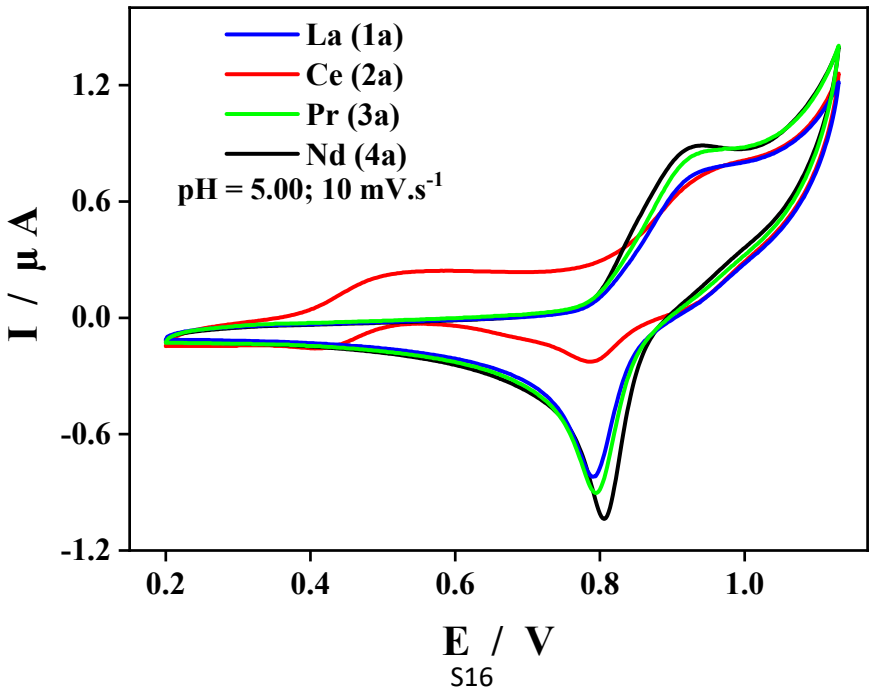

Figure S8. CVs recorded at a scan rate of 10 $mV.s^{-1}$ for all the POMs in the series, studied individually at a concentration of 0.2 mM, in 1.0 M $LiCH_3COO.2H_2O$ + CH_3COOH / pH 5.00.

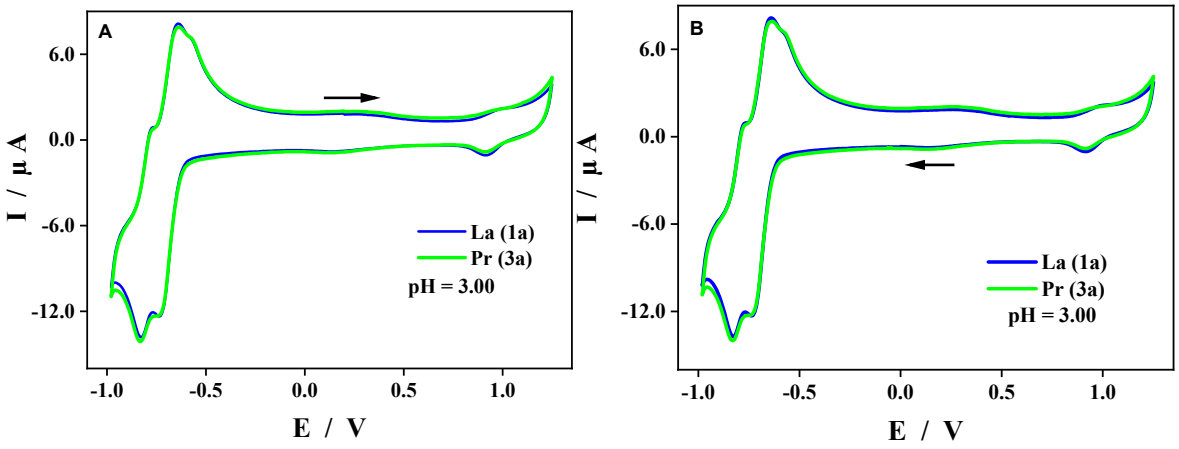

Figure S9. CVs recorded at a scan rate of 100 $mV.s^{-1}$ with La- **(1a)** [blue] and with Pr- **(3a)** [green], studied individually at a concentration of 0.2 mM, in 0.5 M Li_2SO_4 + H_2SO_4 / pH 3.00. (A) Initial scan direction towards the positive potentials. (B) Initial scan direction towards the negative potentials.

Photocatalytic Mechanism:

$POM + hv \rightarrow POM(e^-_{CB} + h^+_{VB})$

$POM(e^-_{CB}) + O_2 \rightarrow POM + \cdot O_2^-$

$\cdot O_2^- + H^+ \rightarrow \cdot HO_2$ *(hydroperoxyl radical)*

$\cdot O_2^- + H^+ + \cdot HO_2 \rightarrow H_2O_2 + O_2$

$2HO_2 \rightarrow H_2O_2 + O_2$

$POM(e^-_{CB}) + H^+ + HO_2 \rightarrow POM + H_2O_2$

$2HO_2 + O_2^- \rightarrow OH + \cdot OH^- + O_2$

$DYE + OH^- \rightarrow$ *degraded product*

$DYE + POM(h^+_{VB}) \rightarrow$ *oxidized product*

$DYE + POM(e^-_{CB}) \rightarrow$ *reduced product*

Figure S10. Proposed Mechanism of Photocatalytic dye degradation

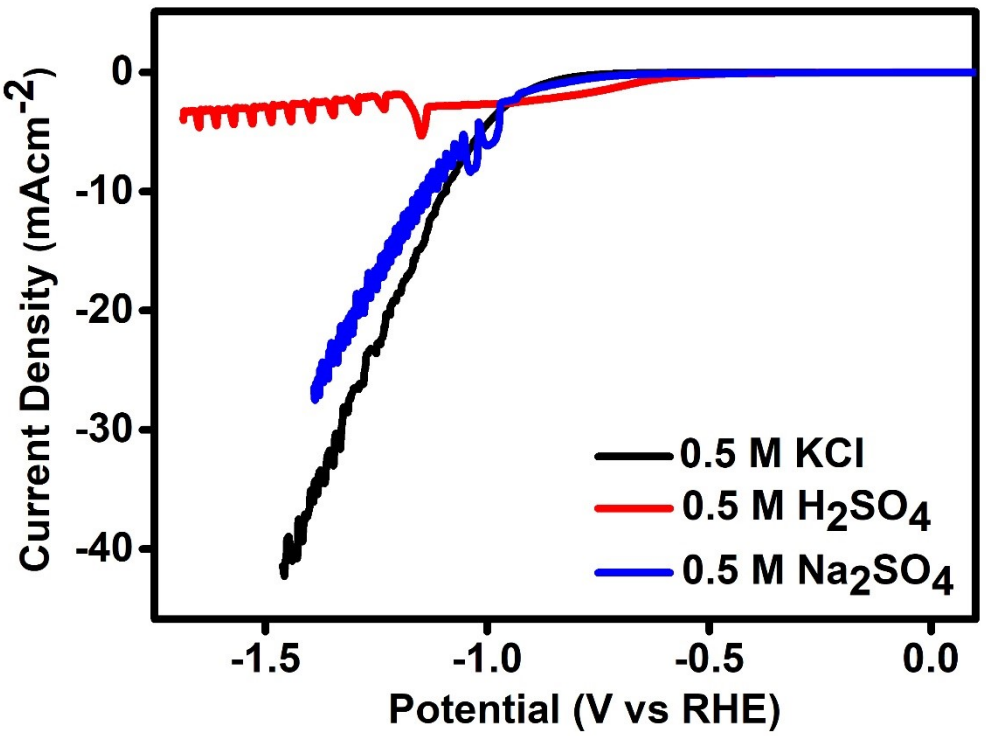

Figure S11. Linear sweep voltammograms for Ce-based POM catalyst in 0.5 M KCl (black), 0.5 M H_2SO_4 (Red), and 0.5 M Na_2SO_4 (Blue).

a)

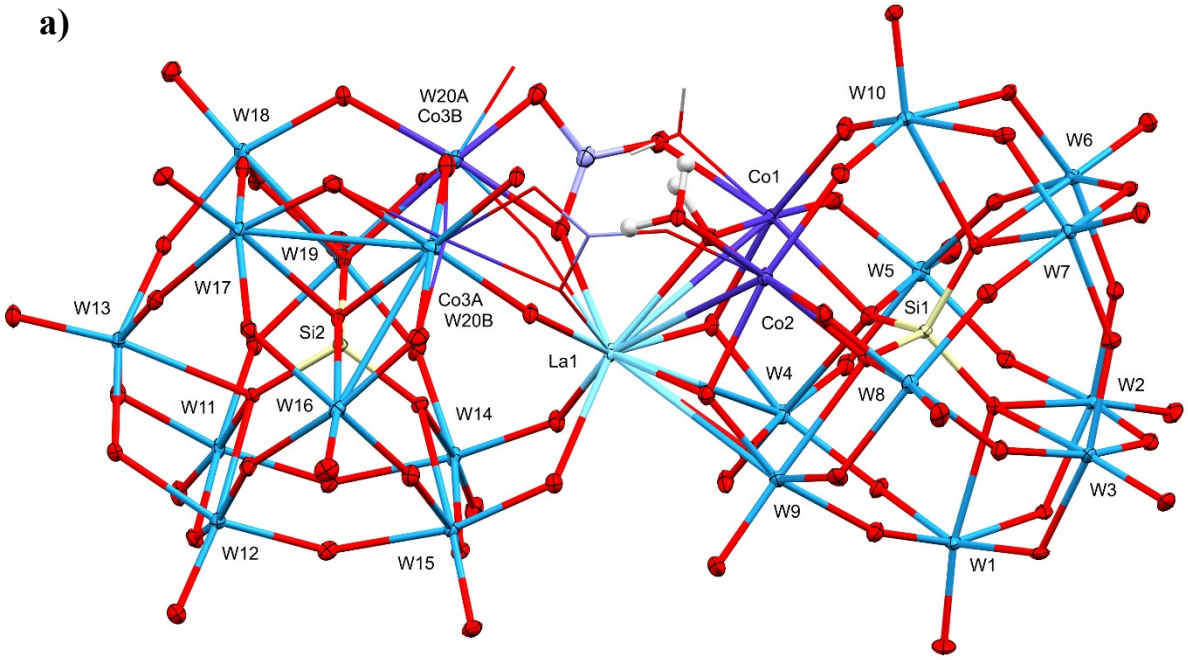
W18
W20A
Co3B
W10
W6
Co1
W19
W17
W5
W7
W13
Co3A
W20B
Si1
Si2
Co2
La1
W4
W8
W2
W11
W16
W14
W3
W9
W12
W15
W1

b)

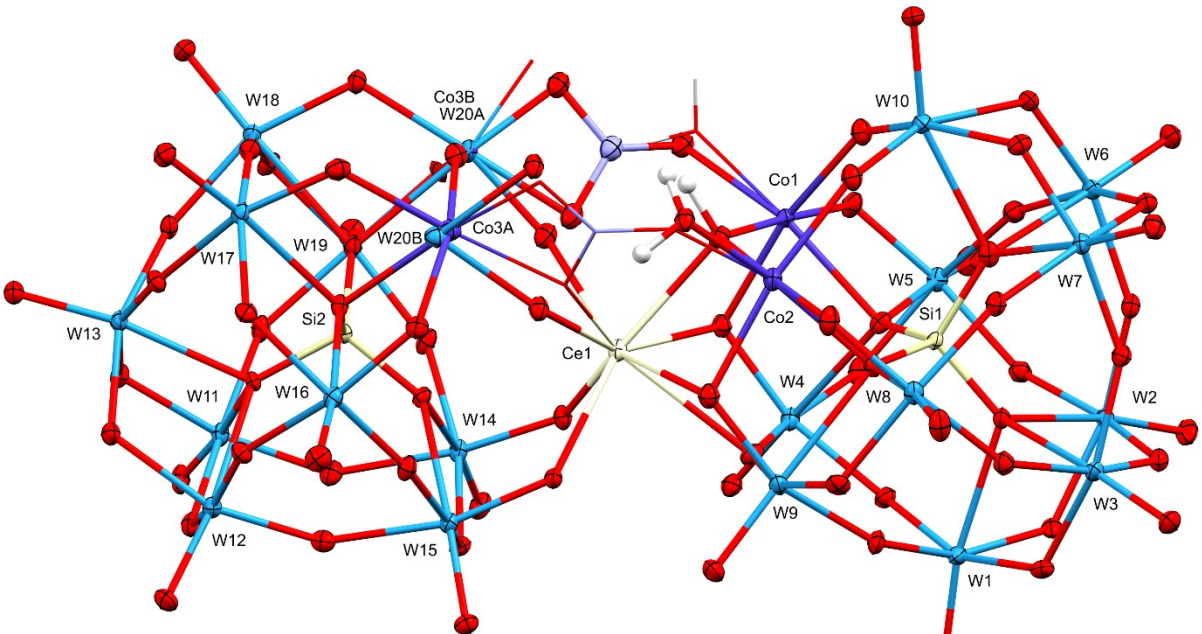
W18
Co3B
W20A
W10
W6
Co1
W19
W20B
Co3A
W17
W5
W7
Si2
Co2
Si1
W13
Ce1
W4
W8
W2
W11
W16
W14
W3
W9
W12
W15
W1

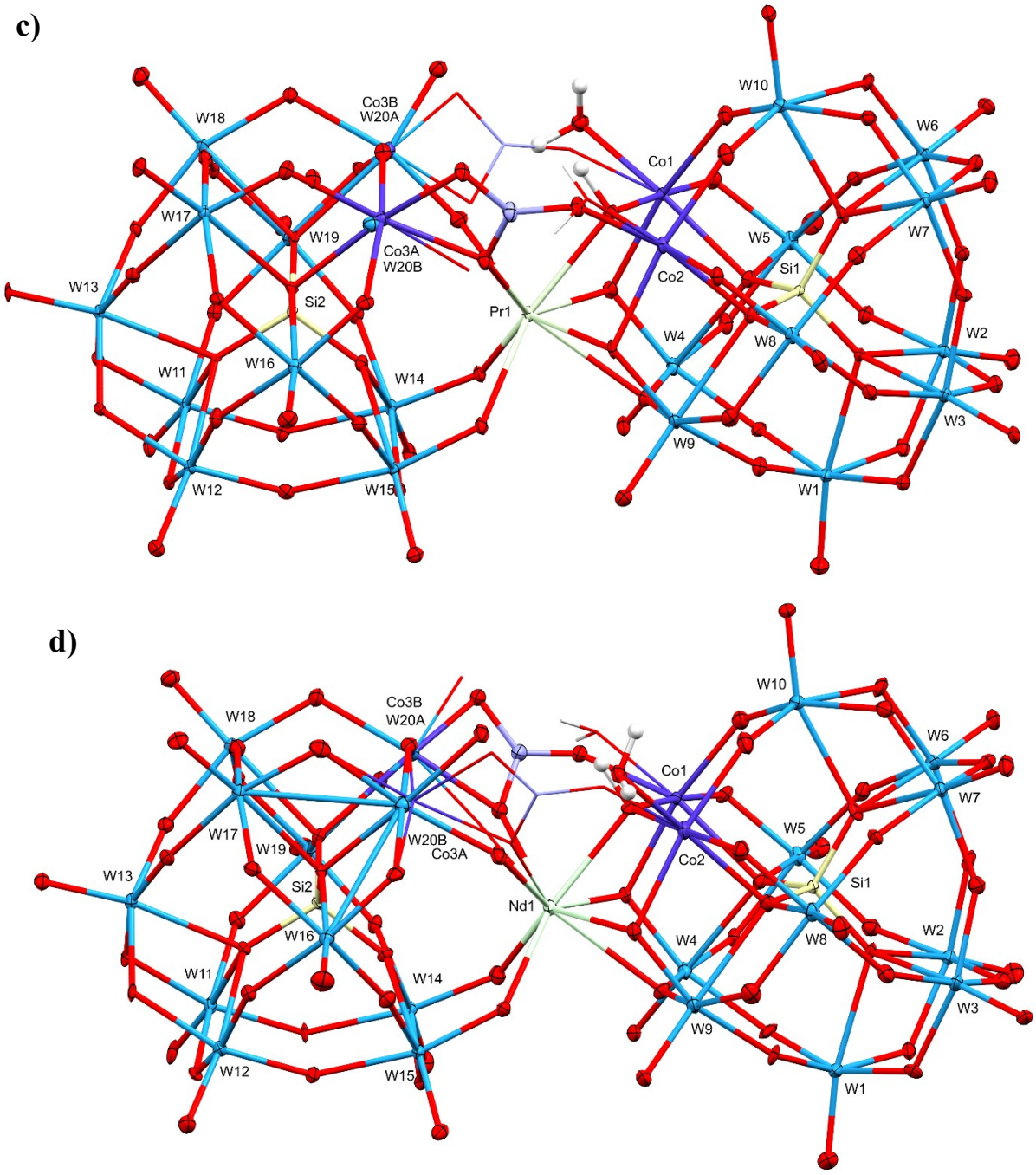

Figure S12. The molecular structures of polyanions: a) **1a**, b) **2a**, c) **3a**, d) **4a** shown without cations (Cs^+, K^+) and isolated water molecules. Displacement ellipsoids are drawn at the 30% probability level.

References

[1] M. A. Fashapoyeh, S. Shokrollahzadeh, A. M. Isloor, and C. Streb, Efficient multi-pollutant removal: The role of Keggin polyoxometalates in polysulfone-chitosan blend membranes, *Int. J. Biol. Macromol.*, **2025**, 311.

[2] H. Malmir, F. M. Zonoz, M. Baghayeri, and R. Tayebee, Synthesis, characterization, and application of mixed-addenda silicon vanado tungstate polyoxometalate integrated into nanoporous MIL-101(Cr) for the quick removal of organic dyes from water, *RSC Adv.*, **2025**, 15, 12, 8918–8930.

[3] W. W. Leow, Facile Synthesis of Hybrid-Polyoxometalates Nanocomposite for Degradation of Cationic and Anionic Dyes in Water Treatment, *Appl. Sci. Eng. Prog.*, 2024.

[4] R. Guo, Construction of ZnO/Keggin Polyoxometalate Nano-heterojunction Catalyst for Efficient Removal of Rhodamine B in Aqueous Solution, *J. Inorg. Organomet. Polym. Mater.*, **2022,** 32, 1599–1615.

[5] D. Pithadia, V. Hegde, V. P. Brahmkhatri, and A. Patel, New catalyst comprising Silicotungstic acid and MCM-22 for degradation of some organic dyes, *Environ. Sci. Pollut. Res.*, **2020**.

[6] Q. Y. Zhai, J. Su, T. T. Guo, J. Yang, J. F. Ma, and J. S. Chen, Two Porous Polyoxometalate-Resorcin arene-Based Supramolecular Complexes: Selective adsorption of organic dyes and electrochemical properties, *Cryst. Growth Des.*, **2018**, 18, 10, 6046–6053.

[7] Y. Zheng, H. Gan, Y. Zhao, W. Li, Y. Wu, X. Yan, Y. Wang, J. Li, J. li and X. Wang, Self-Assembly and Antitumor Activity of a Polyoxovanadate-Based Coordination Nanocage. *Chemistry–A European Journal*, **2019,** *25*(67), 15326-15332.

[8] H. Zhao, L. Tao, F. Zhang, Y. Zhang, Y. Liu, H. Xu, G. Diao, L. Ni, Transition metal substituted sandwich-type polyoxometalates with a strong metal–C (imidazole) bond as anticancer agents. *Chem. Comm.*, **2019,** 55(8), 1096-1099.

[9] Z. Dong, Y. Yang, S. Liu, J. Lu, B. Huang and Y. Zhang, HDAC inhibitor PAC-320 induces G_2/M cell cycle arrest and apoptosis in human prostate cancer, *Oncotarget*., **2017**, 512-523.

[10] I. E. Leon, V. Porro, S. Astrada, M. G. Egusquiza, C.I. Cabello, M. Bollati-Fogolin and S.B. Etcheverry, Polyoxometalates as antitumor agents: bioactivity of a new polyoxometalate with copper on a human osteosarcoma model, *Chemico-biological interactions*, **2014,** *222*, 87-96.